*Annals of Biomedical Engineering*, Vol. 23, pp. 482–490, 1995
Printed in the USA. 

0090–6964/95 $10.50 + .00


# Characterization of the Cellular Microstructure of Ocular Lens Using 2D Power Law Analysis

SHAHRAM VAEZY* and JOHN I. CLARK*,†

Departments of *†Biological Structure and †Ophthalmology, University of Washington, Seattle, WA

**Abstract**—Power law analysis provides a quantitative method for characterization of spatial fluctuations in the cellular microstructure of the ocular lens. In the power law analysis, Fourier components of the spatial fluctuations are computed, and the relationship between the amplitude, $A$, and spatial frequency, $f$, of the components is defined by a power law function: $|A|^2 \approx (1/f)^{\beta}$. The exponent of the function, $\beta$, defines the scaling of the amplitude of the Fourier components as a function of spatial frequency. We performed two-dimensional power law analysis on electron micrographs of lens cells ranging from transparent to opaque. We identified two values of power law exponent, $\beta$, for the spatial fluctuations of all lens cells, one for low- and a second for high-spatial frequencies. In the low-spatial frequency region, the value of $\beta$ was in the range of 0.53 to 1.33, for transparent and opaque cells. In the high-spatial frequency region, the value of $\beta$ increased from 2.78 for transparent lens cells to 3.60 for opaque lens cells. The power law analysis provides a new method for quantitative characterization of the spatial fluctuations in the microstructure of transparent and opaque lens cells.

**Keywords**—Fourier analysis, Transparency, Opacity, Scaling, Cataract

## INTRODUCTION

It is important to characterize the cellular microstructure of the ocular lens because the microstructure is an important measure of the transparent or opaque conditions of the lens. Minimum light scattering in a transparent lens is due to cellular microstructure that contains spatial fluctuations in the refractive index with dimensions small compared with the wavelength of visible light (400–700 nm) (2,3,10,14). Significant light scattering in an opaque lens is due to cellular microstructure that contains spatial fluctuations in the refractive index with dimensions of the order of the wavelength of light.

Figure 1 shows electron micrographs of transparent (Panel a) and opaque (Panel b) mouse lens cells. The spatial fluctuations in the stain density are a measure of the fluctuations in the refractive index because osmium tetroxide and uranyl acetate stain the proteins (11), which comprise 97% of the cytoplasm (9), and the cytoplasmic protein density is proportional to the refractive index (6). The microstructure of transparent cells in Fig. 1a contains a homogeneous distribution of cytoplasmic proteins, resulting in spatial fluctuations with dimensions small compared with the wavelength of light. The microstructure of opaque cells in Fig. 1b contains a heterogeneous network of condensed cytoplasmic proteins, resulting in spatial fluctuations with dimensions of the order of the wavelength of light. In a linescan, which is a plot of stain density across a horizontal line of the micrograph, one can observe the dimensions of the spatial fluctuations, consistent with the expected microstructure of transparent and opaque cells (2,3).

In the micrographs and the linescans, we observe that the spatial fluctuations in the microstructure of the lens cells are not simple fluctuations with obvious dimensions. Instead, these fluctuations are complex and consist of many components. In this paper, we report a quantitative characterization of the spatial fluctuations in the microstructure of lens cells using power law analysis which has proven to be capable of analyzing complex fluctuations (17,20).

Figure 2 demonstrates the power law analysis of two complex fluctuations: white noise (Panel a, top plot) and $1/f$ noise (Panel b, top plot). Using the power law analysis, these fluctuations are characterized by their Fourier spectrum or specifically, the slope of the log-log plot of the spectrum. The middle plots in Fig. 2 are the Fourier spectra of the fluctuations, and the bottom plots are the log-log plots of the Fourier spectra. The Fourier spectrum of the fluctuations is a plot of $|A|^2$ *vs* $f$, where $A$ and $f$ are the amplitude and spatial frequency of the Fourier components, respectively. The log-log plot of the Fourier spectrum is a plot of $\log |A|^2$ *vs* $\log f$. The Fourier spectrum of the white noise is flat, and the log-log plot has a slope of zero. A slope of zero characterizes random white noise fluctuations (20). The Fourier spectrum of the $1/f$ noise decreases as a function of increasing frequency, and the

*Acknowledgments*—We thank Dr. Judy M. Clark for tissue preparation and Mr. Alireza Milaninia for computer programming. This work was supported by Vision Training Grant EY07031, Vision Core Grant EY01730, and Grant EY04542 from the National Eye Institute, a grant from Research to Prevent Blindness Inc., and a grant from the Oculon Corporation.

Address correspondence to S. Vaezy, SM-20, Department of Biological Structure, University of Washington, Seattle, WA 98195.

*(Received 25Mar94, Revised 19Aug94, Revised 29Dec94, Accepted 18Jan95)*

log-log plot has a slope of $-1$. The steeper slope of $1/f$ noise compared with that of the white noise indicates a greater degree of order in the fluctuations of the $1/f$ noise compared with the random fluctuations of the white noise.

A linear log-log plot of the Fourier spectrum is an indication of a power law relationship between the amplitude and frequency of the Fourier components of the fluctuations. Many natural phenomena are observed to have spatial and/or temporal fluctuations with a power law function. Some examples are heart beat (8), myocardial blood flow, (1), ion channel flow (12), colloid aggregation (21), and phase transitions (18). The power law function is a mathematical description of the Fourier spectrum of the fluctuations (16):

$$|A|^2 \approx \left(\frac{1}{f}\right)^{\beta}$$

where $A$ and $f$ are the amplitude and frequency of the Fourier components, respectively, and $\beta$ is the exponent defining the exact form of the power law function (17,20). The exponent, $\beta$, defines the scaling of the amplitude of the Fourier components as a function of frequency, and is equal to the negative of the slope in the log-log plot of the Fourier spectrum ($\log |A|^2$ *vs* $\log f$):

$$\log|A|^2 \approx \beta \log\left(\frac{1}{f}\right) = -\beta \log f.$$

In the above examples, the white noise fluctuation had a slope of zero ($\beta = 0$), and the $1/f$ noise fluctuation had a slope of $-1$ ($\beta = 1$). Complex fluctuations consisting of many components are characterized easily by the power law analysis, yielding characteristic integer or fractional values for $\beta$. The exponent, $\beta$, quantifies the extent of order in the fluctuations. Larger values of $\beta$ represent fluctuations with higher degrees of order. In this paper, we report on the first application of the power law method to the analysis of two-dimensional (2D) spatial fluctuations of the microstructure in transparent and opaque lens cells.

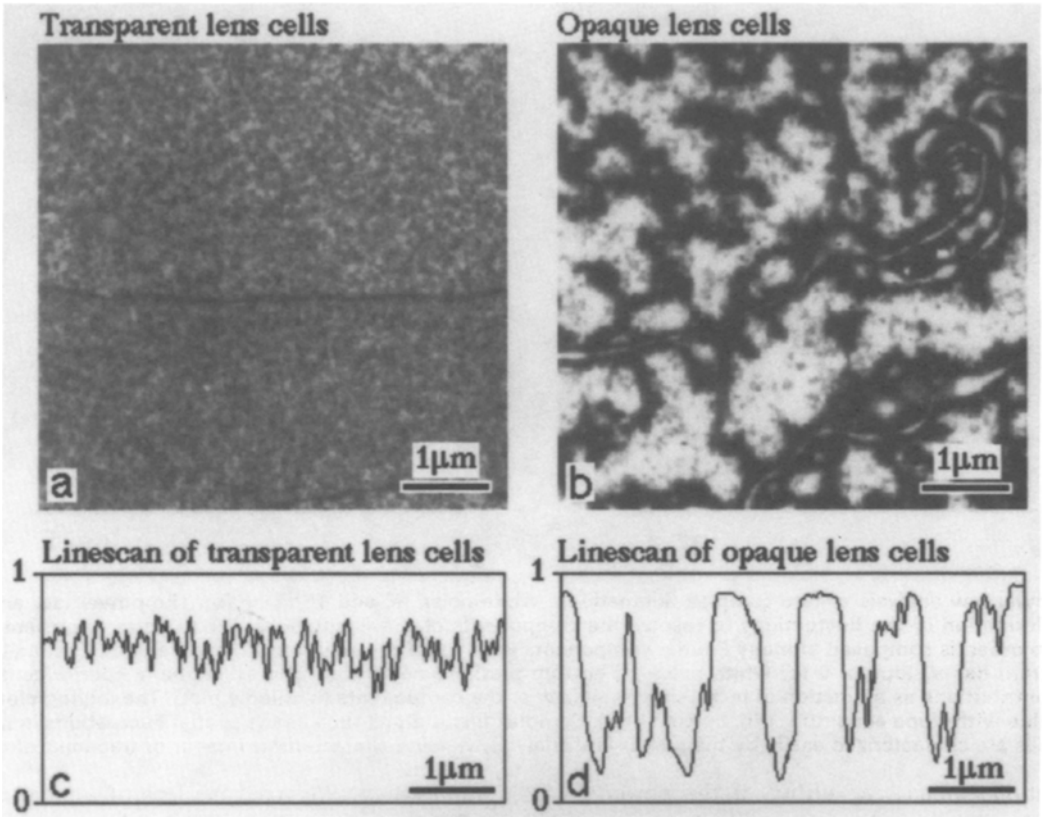


**FIGURE 1. Electron micrographs of transparent (a) and opaque (b) lens cells. The microstructure of transparent cells contains a homogeneous distribution of cytoplasmic proteins, with the spatial fluctuations in microstructure having dimensions much smaller than the wavelength of light. The microstructure of opaque cells contains a heterogeneous distribution of cytoplasmic proteins, with the spatial fluctuations in microstructure having dimensions of the order of the wavelength of light. In the linescans of the micrographs (c from a and d from b) one can observe the dimensions of the spatial fluctuations. The linescans are plots of normalized pixel intensity (0–1) which represents the stain density in the electron micrograph. The micrographs and the linescans demonstrate that the spatial fluctuations in microstructure of the lens cells are complex and composed of many components. Bar = 1 μm.**

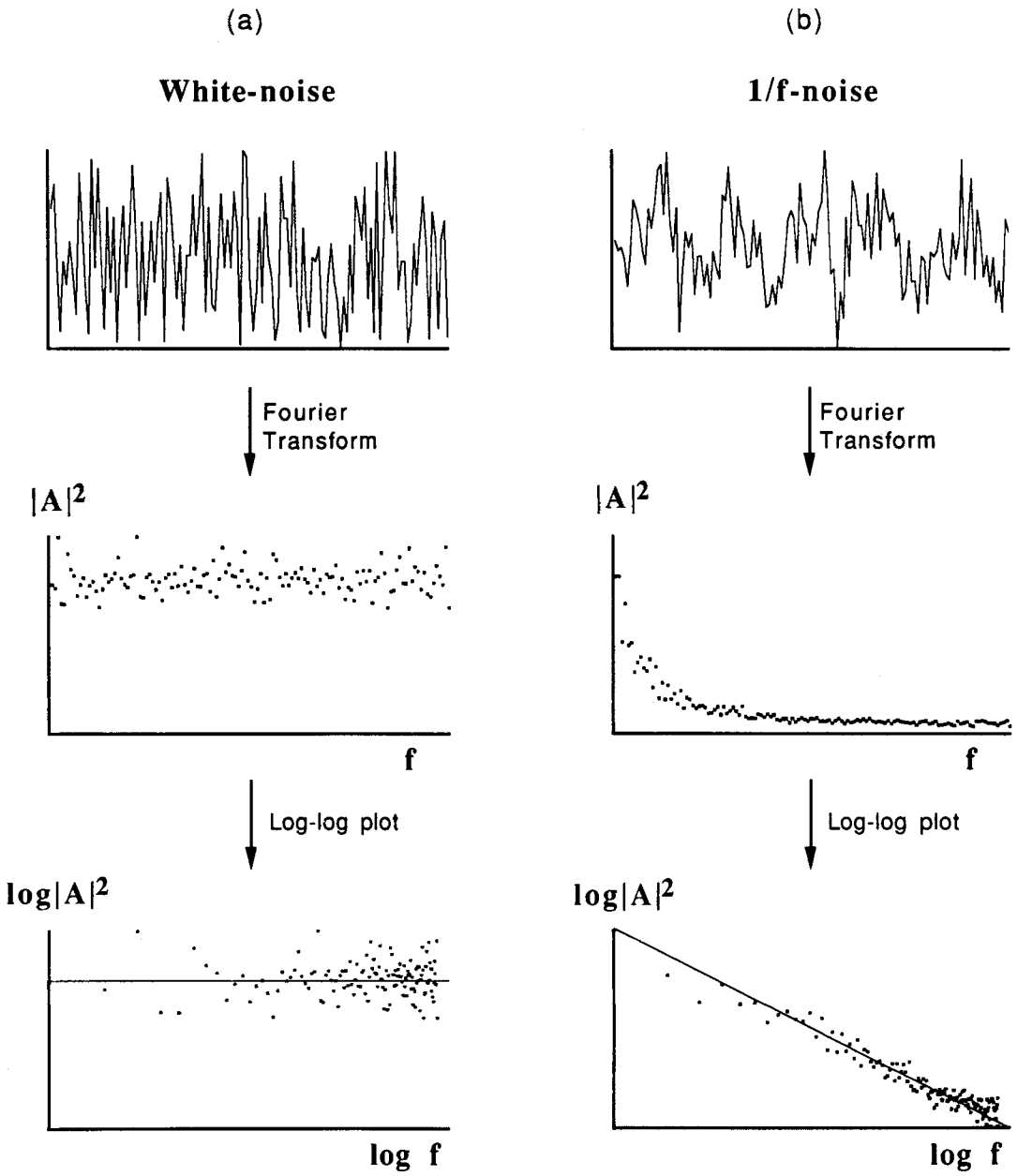


**FIGURE 2. Power law analysis of two complex fluctuations: white noise (a) and 1/*f* noise (b). The power law analysis utilizes Fourier transformation of the fluctuations to resolve the components of the fluctuations. White noise, representing a random signal with no order, is composed of many Fourier components with equal contributions (a, middle plot). The log-log plot of the Fourier spectrum has a slope of 0 for white noise (a, bottom plot). 1/*f* noise is composed of many Fourier components with decreasing contributions as a function of increasing frequency of the components (b, middle plot). The log-log plot can be fitted to a straight line with slope equal to −1 (b, bottom plot). Complex fluctuations such as the spatial fluctuations in microstructure of the lens cells are characterized easily by the power law analysis, yielding characteristic integer or fractional slopes.**

This application extends the utility of the power law method that has been used mostly to analyze temporal fluctuations to the analysis of spatial fluctuations in electron micrographs.

## MATERIALS AND METHODS

The neonatal mouse lens develops a central opacity when its temperature is lowered sufficiently below body temperature. We fixed the lens of a 6-day-old mouse at 25°C, in a solution of 2% glutaraldehyde and 2% paraformaldehyde in 0.1 M Cacodylate buffer of pH 7.4. After 40 hr in the fixative, the anterior and posterior regions of the lenses were cut away leaving a disk that included all the cells from the lens equator to the nucleus. The disks were postfixed in 1% osmium tetroxide for 3 hr at room temperature in the same buffer used for fixation.

They were subsequently stained *en bloc* in 1% uranyl acetate at 37°C for 2.5 hr. The lens tissue was infiltrated and embedded in Poly/Bed 812 epoxy resin (13). A section that contained cells from the lens epithelium (the outer anterior layer) to the center of the lens was used to take electron micrographs of the cells from transparent periphery to opaque center of the lens. Micrographs of the lens cells were taken using JEOL 1200EX electron microscope, in conventional transmission mode, operating at 100 kV, with a magnification of 5,000×. A magnification bar was recorded on the micrograph negative to determine the magnification of each micrograph. The accuracy of the recorded magnification was confirmed using calibration grids. Electron micrographs were printed with the same magnification of those of the negatives (contact sheet prints).

Electron micrographs were digitized using an HP ScanJet Plus scanner at a resolution of 72 pixels per inch and a magnification factor of 300%. These settings resulted in digitized electron micrographs with a magnification of 15,000× (three times that of the printed positives). The range of pixel intensity in the digitized micrographs was 256 levels of gray. The digitized electron micrographs were displayed on a high resolution "Apple" monitor using the application software, "Image" (15) that has been modified in our laboratory to perform the power law analysis. Each digitized micrograph was divided into 6 regions of 256 × 256 pixels that cover the entire micrograph. Each 256 × 256 region was called a region of interest (ROI). All six ROI of each micrograph were analyzed by the power law method. In the digitized micrograph of Fig. 3a the selection of one ROI (Fig. 3b) is shown.

The 2D Fourier spectrum of the ROI was computed (Fig. 3c). The 2D Fourier spectrum is a plot of the squared amplitude of the Fourier components, $|A|^2$, as a function of the spatial frequency, $f$. The amplitude of the Fourier components is represented by the pixel intensity in the Fourier spectrum, on a log scale:

$$\text{Pixel intensity} = \log |A|^2.$$

Pixels with high intensity (dark pixels) represent Fourier components with large amplitude. The pixel intensity (log $|A|^2$) was normalized between 0 and 1. The spatial frequency of the Fourier components is represented by the distance from the center of the Fourier spectrum, in units of $nm^{-1}$. The Fourier components having the lowest spatial frequency were at the center of the 2D Fourier spectrum. The spatial frequency of the Fourier components increased with distance from the center of the 2D Fourier spectrum. The spatial frequency of the Fourier components was within the resolution limits of the ROI, determined by the magnification of the electron micrograph. In the case of the micrographs of the lens, the minimum

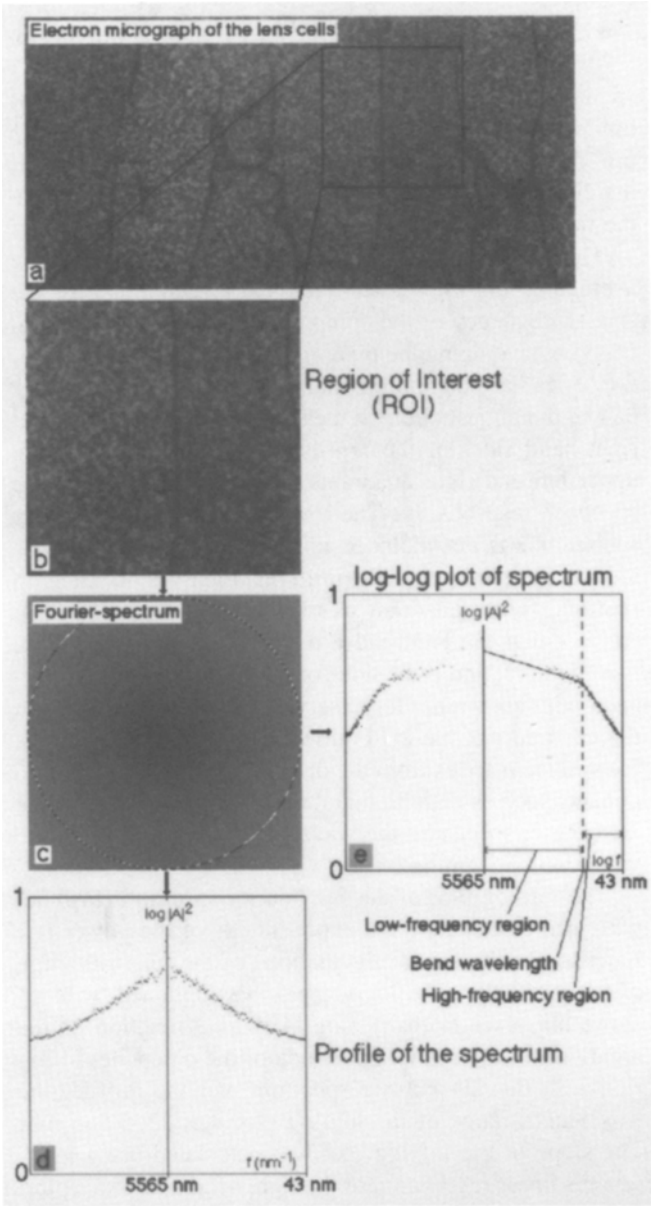


**FIGURE 3. Outline of the method of 2D power law analysis. An electron micrograph of the lens cells was obtained (a). A 256 × 256 pixel region of interest (ROI) of the micrograph was selected for the 2D power law analysis (b). The ROI was Fourier transformed to obtain the 2D Fourier spectrum (c) of the spatial fluctuations in the ROI. In the 2D Fourier spectrum, pixel intensity and pixel position represent amplitude and spatial frequency of the Fourier components respectively. Dark pixels represent large amplitudes. Pixels near the center of the spectrum represent low-spatial frequency, and pixels near the periphery represent high-spatial frequency. The general shape of the Fourier spectrum is represented in a profile of the spectrum (d). The wavelength ranges of the profile and the 2D Fourier spectrum are 43–5,565 nm. The log-log plot of the spectrum (e) is used to determine the power law scaling of the amplitude of the Fourier components as a function of increasing frequency. The slope of the line fitted to the log-log plot is the negative of β, the exponent of the power law function. Two regions having two different power law scaling were found in the 2D Fourier spectra of the lens cells. The low-frequency region is near the center of the plot and the high-frequency region is near the edge of the plot. These two regions are separated by a vertical dashed line which is positioned at the bend wavelength.**

spatial frequency of the Fourier components was (1/43) $nm^{-1}$ and the maximum spatial frequency was (1/5565) $nm^{-1}$. In terms of the wavelength (1/spatial frequency), the 2D Fourier spectrum contained Fourier components in the range of 43–5,565 nm.

The profile of the Fourier spectrum (Fig. 3d) was the average of log $|A|^2$ (pixel intensity) as a function of the spatial frequency of the components. The profile was obtained by averaging the pixel intensity (log $|A|^2$) as a function of radial position (spatial frequency, $f$) in the upper half of the largest circle in the spectrum (19). The left and right hand sides of the profile were the averages of the upper left and right quadrants of the largest circle in the spectrum respectively. The lower half of the 2D Fourier spectrum was not included in the profile because it was identical to the upper half (third quadrant was identical to first and fourth quadrant was identical to second) due to the fact that the ROI had a real part with no imaginary part. The left and right sides of the profile were not averaged with each other to preserve possible asymmetries in the quadrants of the 2D Fourier spectrum. Asymmetry in the spectrum arises from the orientation of structural components such as cellular membranes in the ROI. As in the 2D Fourier spectrum, the wavelength range of the profile was 43–5,565 nm.

The log-log plot of the 2D Fourier spectrum (Fig. 3e) was used to calculate the exponent, $\beta$, of the power law function for the spatial fluctuations of the microstructure of the lens cells. The log-log plot was obtained by averaging the pixel intensity (log $|A|^2$) as a function of the logarithm of the spatial frequency of the components (log $f$). As in the 2D Fourier spectrum and the profile, the wavelength range of the log-log plot was 43–5,565 nm. The slope of the log-log plot was calculated using least-squares linear regression for the right hand side of the plot. The slope of the line fitted to the points of the log-log plot was equal to negative of $\beta$, the exponent of the power law function. In calculating the slope and the value of $\beta$, log $|A|^2$ was not normalized between 0 and 1, to provide a comparison of our value of $\beta$ with those of the literature values.

In the log-log plots for the lens we found two regions with different slopes (Fig. 3e). The slope of a line fitted to the points of the log-log plot in the low-frequency region (close to the center of the plot) was smaller than that of the high-frequency region (close to the edge of the plot). The position on the $x$ axis where the change in the slope was observed was defined as the bend wavelength in the log-log plot. The position of the bend wavelength is indicated by a vertical dashed line in Fig. 3e. The spatial frequency at which the bend occurred was found using the following procedure: an initial correlation coefficient was calculated for fitting a line to 50 points of the highest frequency component. As more points from the low-frequency side were included in calculating the slope, the correlation coefficient was calculated. When the correlation coefficient deviated from the original value by 0.5%, the spatial frequency of the last point included in calculating the slope was defined as the spatial frequency of the bend. The bend wavelength was 1/spatial frequency of the bend.

## RESULTS

The appearance of the lens of a 6-day-old mouse at 25°C is represented in the schematic drawing in Fig. 4. The lens was transparent in the periphery and opaque in the center. The increase in opacity was gradual across the radius of the lens from the periphery to the center. The approximate locations of the five electron micrographs, selected for the 2D power law analysis, are shown by numbered squares. Five representative ROI of the micrographs are shown in Fig. 5. All ROI had the same magnification. ROI 1 shows cells from the most peripheral region of the lens, near the lens epithelium. These cells contained some organelles and their cytoplasm was smooth and homogeneous. ROI 2–5 show cells in progressively deeper regions of the lens. These cells had no large organelles, and were composed mainly of cytoplasmic proteins. From ROI 2 to ROI 5, the microstructure demonstrated a progressive aggregation of cytoplasmic proteins resulting in a heterogeneous distribution of cytoplasmic proteins. Thus, the dimensions of the spatial fluctuations in the cell microstructure increased gradually from ROI 2 to ROI 5. Using the power law analysis we characterized the microscopic spatial fluctuations of the lens cells observed in the electron micrographs.

The 2D Fourier spectra of the five ROI in Fig. 5, and the profiles of the spectra are shown in Fig. 6. All spectra and profiles had the same wavelength range of 43–5,565 nm. In all 2D Fourier spectra, pixels near the center of the spectrum had higher intensities than those near the edge of the spectrum. This general shape of the spectra indicated

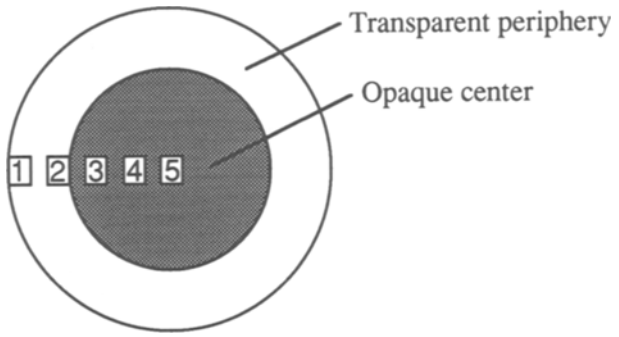


**FIGURE 4. The appearance of the lens of a 6-day-old mouse at 25°C. The lens was transparent in the periphery and opaque in the center. The opacity increased gradually across the radius of the lens. Numbered squares 1–5 represent approximate locations of five electron micrographs taken for the analysis.**

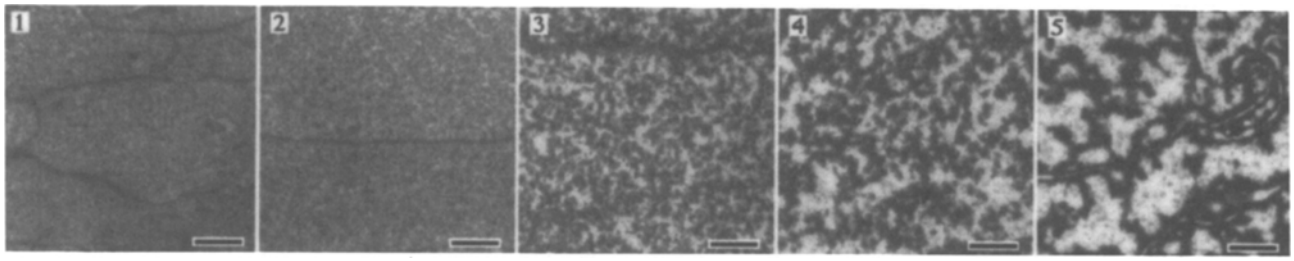


**FIGURE 5. Five representative ROI from the electron micrographs of the lens cells. ROI 1 is from the cells immediately under the lens epithelium, containing organelles and cytoplasmic inhomogeneities. Across the radius of the lens (ROI 2 to 5) there is a gradual increase in the dimensions of the spatial fluctuation in microstructure, due to aggregation of proteins. Bar = 1 μm.**

that the amplitude of the Fourier components decreased as a function of increasing spatial frequency of the components. The decrease in the amplitude of the Fourier components as a function of increasing spatial frequency in each spectrum is demonstrated in the profiles. The profiles demonstrated that the decrease in the amplitude of the Fourier components was not the same for all spectra. Profiles 1 and 2 appeared flatter than profiles 3–5.

Using the log-log plot of the 2D Fourier spectra (Fig. 7), we determined the exponent of the power law function of the spatial fluctuations in microstructure. The exponent is the negative of the slope of the log-log plot. We found that the log-log plot of each spectrum had two regions with two different slopes. The position of the bend wavelength that separated the two regions is indicated by a vertical dashed line in each log-log plot. The slopes of the log-log plots in the low- and high-frequency regions were determined. The results are listed and plotted in Fig. 8. The values in the table of Fig. 8 represent average values based on six different ROI covering the entire area of each electron micrograph. The values in the parenthesis are the standard deviations. The results listed and plotted in Fig. 8 are described below:

(i) In all log-log plots, the slope in the high-frequency region was larger than the slope in the low-frequency region.
(ii) The slopes in the low-frequency regions of plots 2–5 were not different statistically and varied from $-0.95$ to $-0.53$, with a maximum standard deviation of 0.51. In plot 1, the slope in the low-frequency region ($-1.33 \pm 0.19$) was slightly larger than those in plots 2–5.
(iii) The bend wavelength increased from 186 to 1232 nm from plot 1 to plot 5. The standard deviation was approximately 10–15% of the bend wavelength throughout.
(iv) The slope of the log-log plot in the high-frequency region increased gradually from plot 1 to plot 3 ($-2.78$ to $-3.57$), and was approximately constant

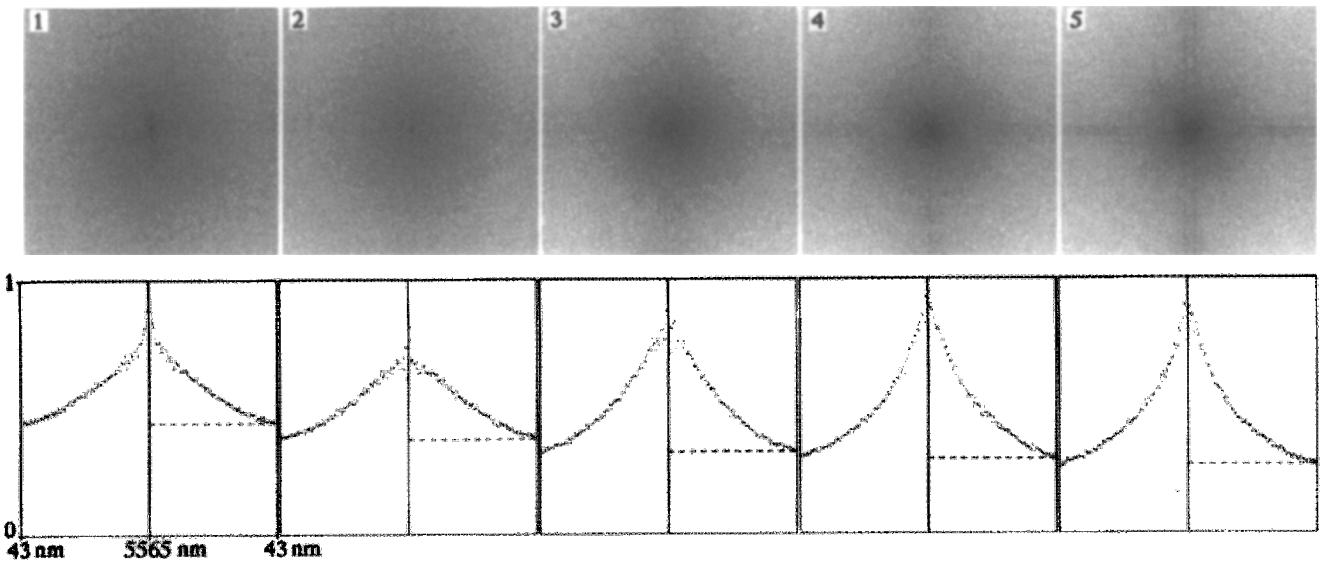


**FIGURE 6. The 2D Fourier spectra of the five ROI in Fig. 5, and profiles of the Fourier spectra. In all spectra the Fourier components near the center of the spectrum have larger amplitude (pixel intensity) compared with those near the edge of the spectrum.**

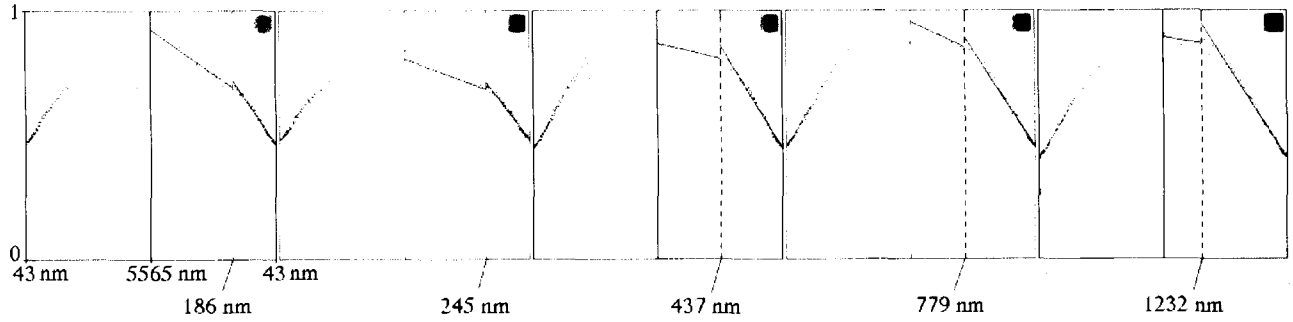


**FIGURE 7. The log-log plots of the five 2D Fourier spectra in Fig. 6. The log-log plots were used to determine the power law scaling of the spatial fluctuations in microstructure. Two regions of different power law scaling were found for each log-log plot: low- and high-frequency regions. For each log-log plot, a line fitted to the points of each region is shown.**

for plots 3–5. The standard deviation in the slope of the high-frequency region decreased generally from plot 1 to plot 5.

## DISCUSSION

Using the 2D power law analysis, we characterized quantitatively the spatial fluctuations in the cell microstructure of the ocular lens. The microstructure of lens cells, ranging from transparent to opaque, was observed in electron micrographs taken across the radius of a mouse lens with a central opacity. The 2D Fourier transformation of the micrographs provided the amplitude, $A$, and the spatial frequency, $f$, of the Fourier components of the spatial fluctuations in microstructure. We found that in the Fourier spectrum of all lens cells the amplitude of the Fourier components decreased as a function of increasing spatial frequency. In all Fourier spectra, the amplitude of the Fourier components was scaled as a power law function: $|A|^2 \approx (1/f)^{\beta}$. The exponent, $\beta$, determined from the slope of the log-log plot of the 2D Fourier spectrum, defined the power law scaling of the amplitude of the Fourier components as a function of the spatial frequency.

All log-log plots of the Fourier spectra of the lens cells demonstrated two regions of power law scaling, separated by a bend. The region extending from 5565 nm to the bend was the low-frequency region, and the region extending from the bend to 43 nm was the high-frequency region. The slope of the log-log plot in the two regions defines the power law scaling of the Fourier components and charac-

Quantitative parameters of the log-log plots

| Log-log plot Number | Low-frequency slope | Bend Wavelength (nm) | High-frequency slope |
|---|---|---|---|
| 1 | -1.33 (± 0.19) | 186 (± 29) | -2.78 (± 0.18) |
| 2 | -0.95 (± 0.26) | 245 (± 19) | -3.03 (± 0.11) |
| 3 | -0.75 (± 0.51) | 437 (± 70) | -3.57 (± 0.04) |
| 4 | -0.60 (± 0.36) | 779 (± 119) | -3.60 (± 0.07) |
| 5 | -0.53 (± 0.45) | 1232 (± 149) | -3.60 (± 0.04) |

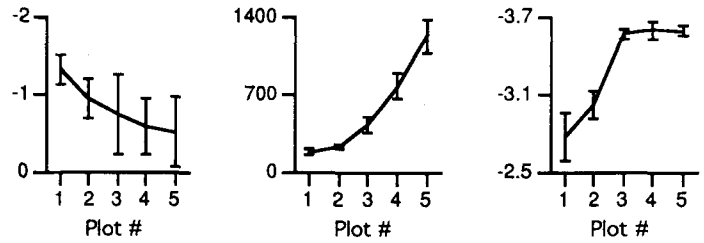


**FIGURE 8. The slopes of the log-log plots in the low- and high-frequency regions and the bend wavelength. The values represent the average values based on six Fourier spectra of six ROI covering the entire area of each electron micrograph. The values in the parenthesis represent the standard deviations. Under each column, the data of the column are plotted as a function of plot number.**

terizes the extent of structural order in the microstructure of the lens cells. As shown in the example of Fig. 2, a slope of zero defines random microstructure and an increase in the slope defines increase in the structural order. In the low-frequency region, the slopes were similar with values $< -1$ for plots 2–5. The close-to-zero value of the slope in the low-frequency region indicates a close-to-random structure of the cytoplasmic protein distributions for dimensions larger than the bend wavelength. Plot 1 had a slope ($-1.33$) slightly steeper than those of plots 2–5, indicating more order in the low-frequency components of ROI 1 compared with ROI 2–5. This difference in the slope is due to presence of organelles in ROI 1 that are not present in ROI 2–5. In fact, using image processing techniques, the organelles in ROI 1 were replaced by protein distributions copied from neighboring cytoplasmic regions and a slope of $-0.95$ was found in the low-frequency region of the log-log plot (not shown), similar to those of ROI 2–5. In the high-frequency region, the slope became steeper in plots 1 to 3 ($-2.78$ to $-3.57$), indicating an increase in the structural order. The increase in the slope for plots 1 to 3 may be due to reorganization in the microstructure of the lens cells in the transition from transparency to opacity. In ROI 1 and 2, there is a homogeneous distribution of cytoplasmic proteins, showing little structural order. In ROI 3, the cytoplasmic proteins condensed into large heterogeneous structures, organized along membranes and as a cytoplasmic network. Plots 3–5 had a similar slope of approximately $-3.57$ to $-3.60$, indicating the similarity in the organization of the microstructure, and specifically the organization of protein aggregates in the opaque lens cells of ROI 3–5.

The value of β has been related to the Hurst coefficient, $H$ (16). In the 2D Fourier spectrum, we have:

$$|A|^2 \approx \left(\frac{1}{f}\right)^{\beta} = \left(\frac{1}{f}\right)^{2H+2}$$

where β is the exponent of the power law and $H$ is the Hurst coefficient. Three distinct categories of $H$ have been discussed by Saupe (16): $H < ½$, $H = ½$, and $H > ½$. $H < ½$ defines negative correlation, indicative of fluctuations with major contributions from high-frequency components. $H = ½$ defines Brownian fluctuations, obtained from integration of white noise in the spatial domain. $H > ½$ defines positive correlation, indicative of fluctuations with major contributions from low-frequency components. In the high-frequency region of the log-log plots we have the values in Table 1.

The three categories of $H$ are represented in plots 1 through 5. Plot 1 has $H < ½$, which indicates a negative correlation in the spatial fluctuations, due to dominant contributions of the high-frequency components resulting from homogeneous distribution of cytoplasmic proteins of the lens cells in ROI 1. Plot 2 has $H \approx ½$, which indicates Brownian spatial fluctuations, due to nonrandom distribution of cytoplasmic proteins in the normal transparent cells. Plots 3–5 have $H > ½$, which indicates a positive correlation in the spatial fluctuations, due to major contributions of low-frequency components introduced by the aggregation of cytoplasmic proteins in abnormal opaque cells. The value of β and the Hurst coefficient may be directly related to the fractal dimension of the lens cell microstructure which might be measured using grid techniques (7).

**TABLE 1. Values of the exponent of the power law, β, and the Hurst coefficient, H, for plots 1–5.**

| Plot # | β | *H* |
|---|---|---|
| 1 | 2.78 | 0.39 |
| 2 | 3.03 | 0.52 |
| 3 | 3.57 | 0.78 |
| 4 | 3.60 | 0.80 |
| 5 | 3.60 | 0.80 |

From log-log plot 1 to 5, the bend shifted to larger wavelengths (Table of Fig. 8), concomitant with the increase in the size of the spatial fluctuations in the microstructure from ROI 1 to ROI 5 (Fig. 5). The bend wavelength may represent a measure of the size of the ordered structures formed in the cytoplasm of the transparent and opaque lens cells. The mean size of the ordered structures, measured using light scattering techniques (5), will provide a basis for quantitative correlation between light scattering and the parameters of the power law analysis. It is interesting that ROI 1 and 2, yielding bend wavelengths of approximately 200 nm, are from the transparent region of the lens, while ROI 3–5, yielding bend wavelengths considerably greater than 200 nm, are from the opaque region of the lens. These results are consistent with the theory of transparency of the eye (2).

The power law analysis has promising applications in the study of microstructure of biological cells and tissues in differentiation, aging, and pathogenesis. The method will provide new quantitative information on structural organization of cytoplasmic and extracellular architecture. The error associated with the power law analysis involves the several steps of the analysis: tissue preparation, electron microscopy, scanning, digitizing, Fourier transformation, and linear regression of the average log-log plots of the 2D Fourier spectra (13,16,17,19). The error associated with tissue preparation was monitored by observing the transparency or opacity of the lens from the periphery to the center. The transparency or opacity are functions of the cell microstructure, and alterations in the microstructure were found to be minimal due to minimum change in transparency or opacity of the lens at different radial positions. The error associated with electron microscopy and scanning were minimized by calibration of the microscope

and selection of an appropriate magnification to prevent aliasing, respectively. The Fourier transformation of the micrograph is an exact mathematical formulation and considered to be free of error as a step in the power law analysis. The error associated with the linear regression of the log-log plots was quantified by the correlation coefficient of the regression. The correlation coefficients for high-frequency slopes were in the range of 0.98–0.99, increasing from plot 1 to plot 5. The correlation coefficients for low frequency slopes were in the range of 0.89–0.37, decreasing from plot 1 to plot 5. The changes in the value of the correlation coefficient were due to the progressively larger number of points in the high-frequency region, and smaller number of points in the low-frequency region, from plot 1 to plot 5. The standard deviation of the slope is an indirect measure of the correlation coefficient, decreasing in the high-frequency region, and increasing in the low-frequency region in plots 1–5, respectively.

In this paper, we presented the first characterization of the lens cell microstructure using 2D power law analysis. The Fourier components of the spatial fluctuations in microstructure of the lens cells follow a power law function: $|A|^2 \approx (1/f)^{\beta}$, in two regions of the low- and high-spatial frequency. The power law scaling in the two regions was found for the lens cells ranging from transparent to opaque. We are currently researching the specific characteristics of the lens microstructure that are responsible for the low- and high-spatial frequency regions and the measured power law scaling in these regions. We expect the power law analysis to have numerous applications in quantitative evaluations of cell and tissue microstructure.

## REFERENCES


1. Bassingthwaighte, J. B., R. B. King, and S. A. Roger. Fractal nature of regional myocardial blood flow heterogeneity. *Circ. Res.* 65(3):578–590, 1989.
2. Benedek, G. B. Theory of the transparency of the eye. *Appl. Opt.* 10:459–473, 1971.
3. Bettelheim, F. A. Synersis and its Possible role in cataractogenesis. *Exp. Eye Res.* 28:189–197, 1979.
4. Clark, J. I., and G. B. Benedek. Phase diagram for cell cytoplasm from the calf lens. *Biochem. Biophys. Res. Commun.* 95(1):482–489, 1980.
5. Delaye, M., J. I. Clark, and G. B. Benedek. Identification of the scattering elements responsible for lens opacification in cold cataract. *Biophys. J.* 37:647–656, 1982.
6. Delaye, M., and A. Gromiec. Mutual diffusion of crystalline proteins at finite concentrations: a light scattering study. *Biopolymers* 22:1203–1221, 1983.
7. Feder, J. Fractals. New York: Plenum Press, 1988, pp. 6–30.
8. Goldberger, A. L., V. Bhargava, B. West, and A. J. Mandell. On a mechanism of cardiac electrical stability: the fractal hypothesis. *Biophys. J.* 48:525–528, 1985.
9. Harding, J. J., and M. J. C. Crabbe. The lens: development, proteins, metabolism and cataract. In: *The Eye,* vol. 1B, edited by H. Davson. Orlando: Academic Press, 1984, pp. 207–492.
10. Hart, R. W., and R. A. Farrell. Light scattering in the cornea. *J. Opt. Soc. Am.* 59:766–774, 1969.
11. Hayat, M. A. Principles and Techniques of Electron Microscopy, Biological Applications, vol. 1. New York: Van Nostrand Reinhold, 1970, pp. 183.
12. Liebovitch, L. S., and T. I. Toth. Fractal activity in cell membrane ion channels. *Ann. N.Y. Acad. Sci.* 591:375–391, 1990.
13. Luft, J. H. Improvements in epoxy resin embedding methods. *J. Biophys. Biochem. Cytol.* 9:409–414, 1961.
14. Philipson, B. Changes in the lens related to the reduction of transparency. *Exp. Eye Res.* 16:29–39, 1973.
15. Rasband, W. *Image Version 1.21, User's Guide.* Bethesda: National Institute of Health, PB90-123308, 1989.
16. Saupe, D. Random fractals in image synthesis. In: *Fractals and Chaos,* edited by A. J. Crilly, R. A. Earnshaw, and H. Jones, New York: Springer-Verlag, 1991, pp. 89–118.
17. Schepers, H. E., J. H. G. M. van Beek, and J. B. Bassingthwaighte. Four methods to estimate the fractal dimension from self-affine signals. *IEEE Eng. Med. Biol.* 11:57–64, 1992.
18. Stinchcombe, R. B. Fractals, phase transitions and criticality. In: *Fractals in the Natural Sciences,* edited by M. Fleichmann, D. J. Tildeseley, and R. C. Ball. Princeton: Princeton University Press, 1989, pp. 17–33.
19. Vaezy S., J. I. Clark, and J. M. Clark. Quantitative analysis of the lens cell microstructure in selenite cataract using a two-dimensional Fourier analysis. *Exp. Eye Res.* 60:245–255, 1995.
20. Voss, R. F. Fractal in nature: from characterization to simulation. In: *Science of Fractal Images,* edited by H. O. Peitgen, and D. Saupe. New York: Springer-Verlag, 1988, pp. 21–70.
21. Weitz, D. A., and M. Y. Lin. Dynamic scaling of cluster-mass distributions in kinetic colloid aggregation. *Phys. Rev. Lett.* 57(16):2037–2040, 1986.